Jorge G. Cham

Jonathan K. Karpick

Mark R. Cutkosky

Center for Design Research
Stanford University
Stanford, CA 94305-2232, USA
contact: *jgcham@cdr.stanford.edu*

Stride Period Adaptation for a Biomimetic Running Hexapod

Abstract

We demonstrate an adaptation strategy for adjusting the stride period in a hexapedal running robot. The robot is inspired by discoveries about the self-stabilizing properties of insects and uses a sprawled posture, a bouncing alternating-tripod gait, and passive compliance and damping in the limbs to achieve fast (over 4 body-lengths per second), stable locomotion. The robot is controlled by an open-loop motor pattern that activates the legs at fixed intervals. For maximum speed and efficiency, the stride period of the pattern should be adjusted to match changes in terrain (e.g. slopes) or loading conditions (e.g. carrying an object). An ideal adaptation strategy will complement the design philosophy behind the robot and take advantage of the self-stabilizing role of the mechanical system. In this paper we describe an adaptation scheme based on measurements of ground contact timing obtained from binary sensors on the robot's feet. We discuss the motivation for the approach, putting it in the context of previous research on the dynamic properties of running machines and bouncing multi-legged animals, and show results of experiments.

1. Introduction

We have built a family of hexapedal robots that are inspired by discoveries concerning the locomotion of insects and, in particular, of the cockroach. These animals run rapidly (between 10 and 50 body-lengths/second depending on the species) and over rough terrain using a combination of open-loop muscle activation patterns and "preflexes," that is, passive mechanisms that stabilize the animals' motion in response to perturbations (Ahn and Full, 1997; Full et al., 1998; Kubow and Full, 1999; Meijer and Full, in press). Like the insects that inspired them, the robots employ passive mechanical properties that enable them to run quickly (over 4 body-lengths per second) and over hip-height obstacles (see Fig. 1) without closed-loop control (Cham et al., in press; see also multimedia Extensions 1 and 2). Although this approach works well in the laboratory, there is a question about its versatility. How effectively can a particular open-loop control and set of mechanical properties function over a range of conditions that may include variations in ground slope and hardness and changes in loading? Furthermore, the animals or robots themselves may change over time. A limb may become damaged or the mechanical properties may vary with temperature. A way to address this problem is adaptation, in which the parameters of the open-loop control are automatically adjusted to optimize performance as conditions change.

Figure 2 illustrates an approach in which adaptation is combined with preflexes for stable running. An open-loop, feed-forward, motor controller generates the pattern of actuator commands to achieve a steady alternating-tripod gait. The kinematic arrangement and passive compliance and damping of the limbs achieve the locomotion and provide stable response to perturbations. Sensory information is used at a slower rate to adapt, or tune, the motor pattern in response to changing conditions. In running insects, an important reason for relying on preflexes in combination with slow adaptation is that neural conduction speeds are too slow for feedback control to act effectively within each stride period. In robots, of course, the same limitation does not necessarily apply. However, for small and inexpensive robots like our prototype, "Sprawlita," the same approach allows the use of simple sensors without concerns that actuator delays, sensor noise or even failures will jeopardize short-term preformance. This is an important consideration because many sensors become noisy when mounted on a small hexapod running at 7-10 Hz.

The basic design of the Sprawl family of hexapods consists of a body and legs built up in layers using a rapid-prototyping process called Shape Deposition Manufacturing. The design and manufacturing are detailed in Cham et al. (in press) and in Bailey et al. (1999). Each leg has two degrees of freedom but only the thrust direction is actuated, using pneumatic pistons embedded in the legs. When running, hip rotations are passive and are accomplished by flexures of visco-elastic material. This design is inspired by the trochanter-femur joint in cockroaches, which is believed to be mostly passive in the sagittal plane. A servomotor at each hip is used only to establish the equilibrium position of the hip joint. Binary contact sensors are attached to the feet. Pneumatic solenoid valves regulate air-flow into the leg pistons from a high-pressure source. The original Sprawlita design uses two valves, one for each tripod of legs, embedded in the body of the robot. These on/off valves are activated according to an open-loop binary motor pattern. A newer design has a valve embedded in each leg, which results in faster actuator dynamics and more control over the timing of the thrust force at each foot. As will be seen in the following sections, these are important considerations. Depending on configuration, the robots weigh between 0.25-0.33 Kg and have a length of 10-15cm. Maximum speeds range from 0.5-0.8m/sec with preferred stride frequencies of 7-10 Hz.

The operational parameters that can be varied are the stride period (length of time between activation of each tripod) and the duty cycle (length of time that the valves are kept open during each stride) of the motor pattern and the equilibrium positions of the compliant hip joints. All of these parameters contribute to running performance and could be subject to adaptation. In this paper, we focus on stride period and duty cycle.

Figure 3 shows the robot's speed as a function of ground slope for two different stride frequencies, and illustrates the

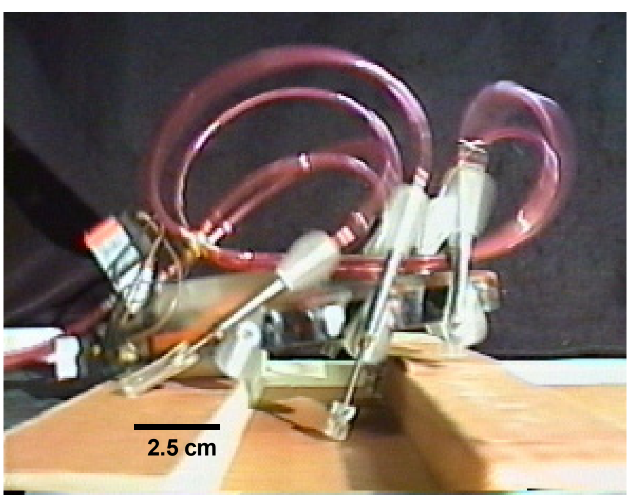

Figure 1. The hexapedal robot has a body and legs fabricated by Shape Deposition Manufacturing (Cham et al., in press) and features embedded actuators and compliant legs. Here the robot is crossing a hip-height obstacle without using sensory feedback and without significantly slowing down or being knocked off course.

importance of adjusting the stride frequency to changing conditions. On level ground the fastest locomotion is obtained with a frequency of approximately 10 Hz. But on a 20 degree slope, locomotion is considerably faster at 5 Hz than at 10 Hz. The optimal frequency also varies somewhat from one robot to the next due to manufacturing tolerances and variations in the materials properties of the legs. Consequently, there is a motivation to make the robots "self-tuning" over a range of operating conditions. Ideally, we would like an adaptation strategy that does not require adding expensive or complicated sensors to the robot.

For these reasons, we examined the relationship between ground contact times (obtained from binary sensors in the robots' feet) and the timing parameters (frequency and duty cycle) of the open-loop motor control. As will be discussed in Section 3, of the various timing quantities that we can examine, the interval between end of thrust (closing of the pneumatic valve) and liftoff of the feet is a good indicator for adjusting the stride frequency. To better understand why this approach works, we first examine a simplified one-legged vertical hopper model.

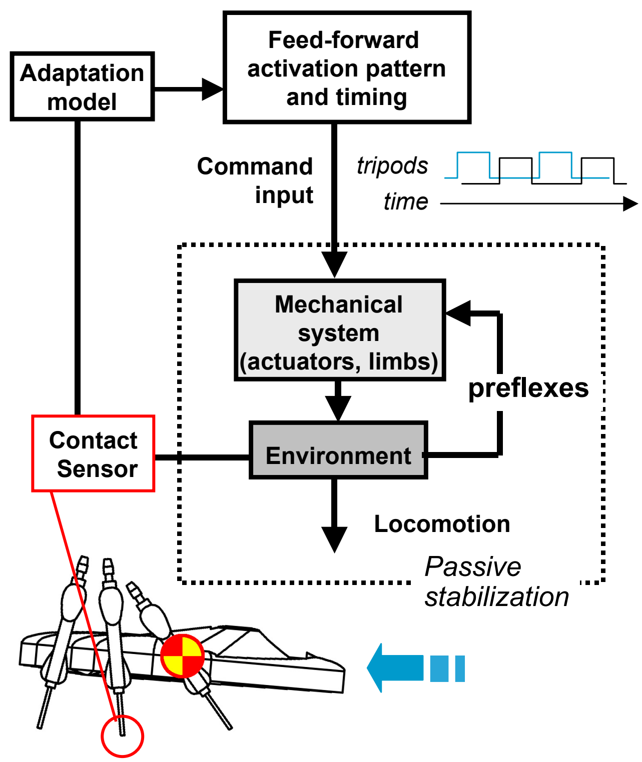

Figure 2. A combination of stabilizing passive mechanisms, or "preflexes," and sensor-based adaptation of an open-loop feed-forward controller provides insects and small robots with a robust, stable and versatile approach to running over rough terrain.

2. Simplified Model for Open-Loop Locomotion and Adaptation

To understand how monitoring the ground contact time can provide information to the robot about the effectiveness of its current motor pattern in running, we start with a simple vertical hopping model that has been frequently utilized in the literature. Although this model cannot tell us about the coupling between vertical and horizontal motion, an important factor in the dynamics of the Sprawl robot family, it does shed light on the relationship between system energy and actuator timing. It provides insight into the circumstances under which a stable, steady-state hopping cycle is achieved with an open-loop control scheme and it helps us determine how to get the most work out of our actuators using only simple sensors.

Variations on this basic model have been examined by several investigators, including Raibert (1986), Koditschek and Buehler (1991), Ringrose (1997), and Berkemeier and Desai (1998). Despite its apparent simplicity, the one-legged vertical hopper exhibits a rich set of dynamic behaviors including stable and unstable periodic motion.

Raibert’s hopper (Raibert, 1986) uses a double-acting pneumatic cylinder and an actuated hip to produce forward motion. The cylinder acts as an air spring when its valves are closed, providing a system similar to the simplified hopper of Figure 4, although with a non-linear spring. Thrust is applied in a closed-loop fashion when the leg is sensed to be at maximum compression. Vertical and horizontal motions are assumed to be decoupled and height is varied by changing the thrust duration. The stability of a simplified one-DOF hopper model based on this closed-loop thrust activation is analyzed by Koditschek and Buehler (1991).

Ringrose (1997) showed that a vertical hopper can maintain stable hopping without sensory feedback, using a linear actuator in series with a spring, and a damper in parallel with the actuator/spring combination. For analysis, Ringrose uses a simplified model in which thrust is applied through an impulsive change in leg length at fixed intervals in time such that thrust initiation occurs before maximum compression of the spring.

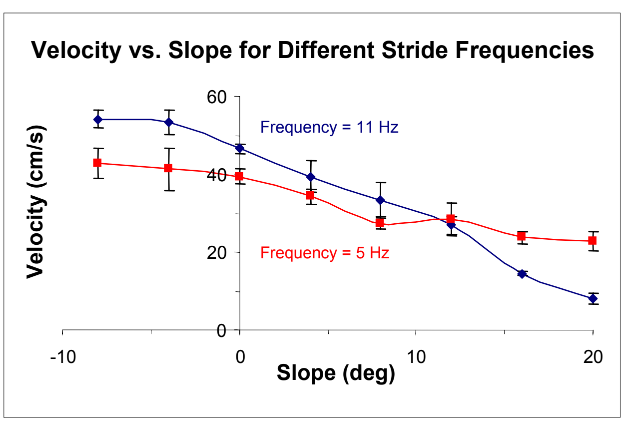

Figure 3. Robot ground speed versus terrain slope for two different stride frequencies. As shown, the optimal stride frequency for maximum speed depends on the slope, which illustrates the need for adaptation.

Berkemeier and Desai (1998) compare Raibert’s method of applying thrust at maximum compression, Ringrose’s open loop control, and a proposed “adaptive periodic forcing” method that adjusts the period of the open loop control based on the velocity at the time that thrust is applied. In their analysis, they use a hopper with a spring and damper in parallel and an actuator that changes the neutral point of the spring. Their analysis shows that their hopper reaches maximum hopping height when the force is applied at maximum spring compression. Using perturbation methods that assume low values of damping, they also show that the motion is stable, without feedback, when the force is applied prior to the maximum compression of the spring and unstable when the force is applied after the maximum compression.

Komsuoglu and Koditschek (2000) analyze the stability of a similar open-loop one-DOF hopper in which thrust is effected by clock-driven changes in stiffness and find conditions for stability, which include the necessary presence of viscous friction.

The physical implementation of the Sprawl robots requires that the minimal damping assumptions made in previous models be reconsidered. In insects, and in the Sprawl family of robots, viscoelastic materials dissipate substantial amounts of energy per cycle. Typical dimensionless damping ratios are on the order of $\zeta = 0.3$ (Garcia et al., 2000). Additionally, a model was needed to determine the practi-

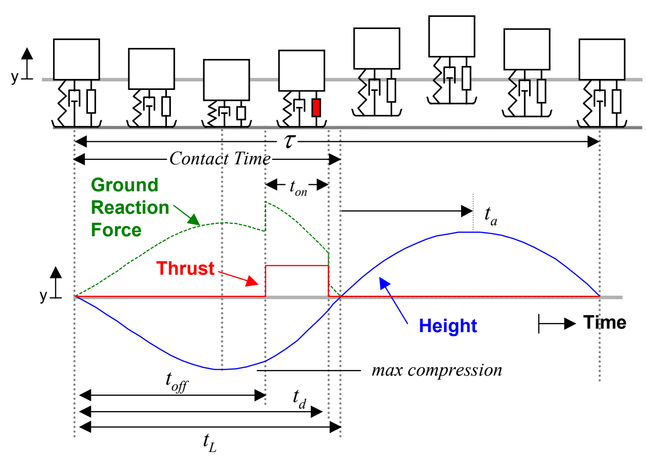

Figure 4. Time history of a single degree-of-freedom vertical hopper. The mass is attached to a massless leg with stiffness k and damping b. After some time t_{off}, a thruster in parallel applies a thrust force, f. At some time t_L, the mass lifts off the ground and travels ballistically in the air.

cality of using a simple binary switch for feedback instead of more complicated and noise-susceptible velocity sensors.

We therefore consider a single-legged vertical hopper which can include substantial viscous damping. Figure 4 depicts a sample time history of this hopping model. The massless leg has stiffness, *k*, damping, *b*, and an actuator that is able to provide a thrust force *f(t)* that is initiated after some time t_{off} and terminated after a fixed duration, t_{on}, or by liftoff, whichever occurs first. The stride period begins at *t=0* as the robot touches down, which occurs when *y=0*, the spring's neutral length. During the ground contact phase, the ground reaction force is given by:

$$GRF = ky + b\dot{y} - f(t) \tag{1}$$

The equation of motion for the mass is:

$$m\ddot{y} = -ky - b\dot{y} - g + f(t) \tag{2}$$

Liftoff occurs when the ground reaction force is equal to zero, and the hopper transitions to an airborne phase, where it travels ballistically. In the next two sections, we consider the conditions for optimal hopping height of this model, and conditions for the existence of stable behavior.

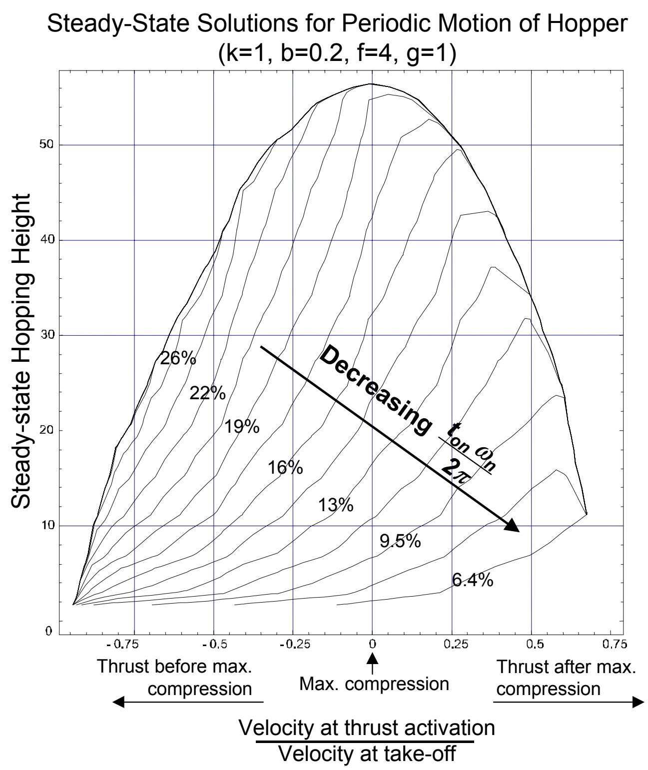

Figure 5. Hopping height as a function of normalized velocity at thrust application for the one-DOF hopper. Each line represents the solutions to the steady-state constraint equations for a given set of operating parameters and thrust duration.

2.1 Optimal hopping height

In steady-state, the landing velocity of one cycle must equal the landing velocity of the previous cycle. Simulations were conducted to determine which values of force application delay, t_{off}, and force duration, t_{on}, meet steady state conditions for given values of *m*, *k*, *b*, *g*, and force *f*. Each solution pair (t_{off}, t_{on}) corresponds to a steady-state hopping cycle with a given steady-state hopping height. Figure 5 shows the steady-state hopping height of these solutions plotted against the velocity at which thrust is initiated for *m=g=k=1*, *b=0.2*, and *f=4* and for a range of thrust durations. The velocity at thrust activation on the horizontal axis of the figure is normalized by the velocity at take-off for each steady-state solution. This normalized velocity is zero if thrust is initiated at maximum compression, approaches -1 if thrust is initiated at landing, and approaches +1 if thrust is initiated near take-off. Each line represents the set of solutions for a given thrust duration t_{on}, here specified as a percentage of the natural period $(2\pi)/w_n$.

Figure 5 shows that for thrust durations greater than 20% of the natural period, peak hopping height is achieved when the thrust is applied near the point of maximum spring compression, that is, when the velocity at activation is nearly zero. For shorter thrust durations, however, optimal steady-state heights occur when thrust is initiated *after* maximum spring compression (velocity at force application is positive).

In evaluating the conditions that determined the maximum hopping heights in Figure 5, it is seen that, for a given force level and duration, hopping height is maximized at the steady-state solution in which the net positive work performed by the actuator within a stride is maximized:

$$\int_{t_{off}}^{(t_{off}+t_{on})} f(t) \cdot \dot{y}(t)dt = WorkInput \tag{3}$$

If *f(t)* is constant, then, for a long thrust that is applied until the end of the ground contact phase, this integral is maximized when thrust activation coincides with maximum compression. For a short thrust duration which ends before the end of the ground contact phase, the conditions for the maximization of this integral are more complex but can be shown to roughly coincide with maximizing the upward velocity at thrust activation (while still achieving end-of-thrust before lift-off).

2.2 Stability and multiple solutions

The plot in Figure 5 shows an example set of solutions to the steady-state constraint equations, regardless of whether thrust is initiated through open- or closed-loop control. Since our hexapedal robots are controlled open loop, we now consider the one-DOF case in which thrust is initiated at fixed intervals of time as dictated by the stride period of the activation pattern. In this case, the system will either converge to one of the steady-state solutions from Figure 5, converge to more complicated hopping patterns, or assume non-periodic behavior. In practice, as we varied the open-loop timing parameters, we found that the simulations converge to different steady-state behaviors, and often don't converge to periodic motion at all. To study the effects of changing the timing parameters on behavior and stability, we considered the local stability of the steady-state solutions.

The steady-state motion of the hopper model is determined by its return map:

$$X_{n+1} = F(X_n) \tag{4}$$

which relates the state after one cycle, X_{n+1}, to the previous state, X_n, for a given set of operating conditions (Sastry, 1999). Steady-state solutions satisfy:

$$X^* = F(X^*) \tag{5}$$

and are called "fixed points." Although the equations of motion that govern the ground-contact and airborne phases are linear, the transitions between the two phases make the return map non-linear and, in this case, intractable to solve explicitly. The local stability of each existing solution is given by the linearized return map, a Jacobian matrix, M, defined as:

$$\delta X_{n+1} = M(X_n)\delta X_n \tag{6}$$

where,

$$M(X_n) = \frac{\partial}{\partial X_n}F(X_n) \tag{7}$$

If the eigenvalues of the matrix M evaluated at the fixed point are within the unit circle, then the fixed point is locally stable, since $M(X^*)$ maps disturbances about the fixed point from one cycle to the next (Sastry, 1999):

$$|eig(M(X^*))| < 1 \tag{8}$$

The return map and the matrix M were found analytically for our one-DOF model using the simplifying assumption that lift-off occurs when $y=0$. With this assumption, the presence of damping in the leg model may cause the ground reaction force to be negative for a short period of time. However, this assumption was found to cause only small differences in the steady-state solutions for the range of damping and mass values used here. The two cases considered in this analysis were: a) when thrust application ends at or after lift-off (termed "Long Thrust"); and b) when thrust application ends before lift-off (termed "Short Thrust"). The analytical equations used in the following results are found in the Appendix.

Figure 6 shows a typical example of the effects of changing the open-loop stride period for the "Long Thrust" case with a given thrust magnitude, f, natural frequency, w, and

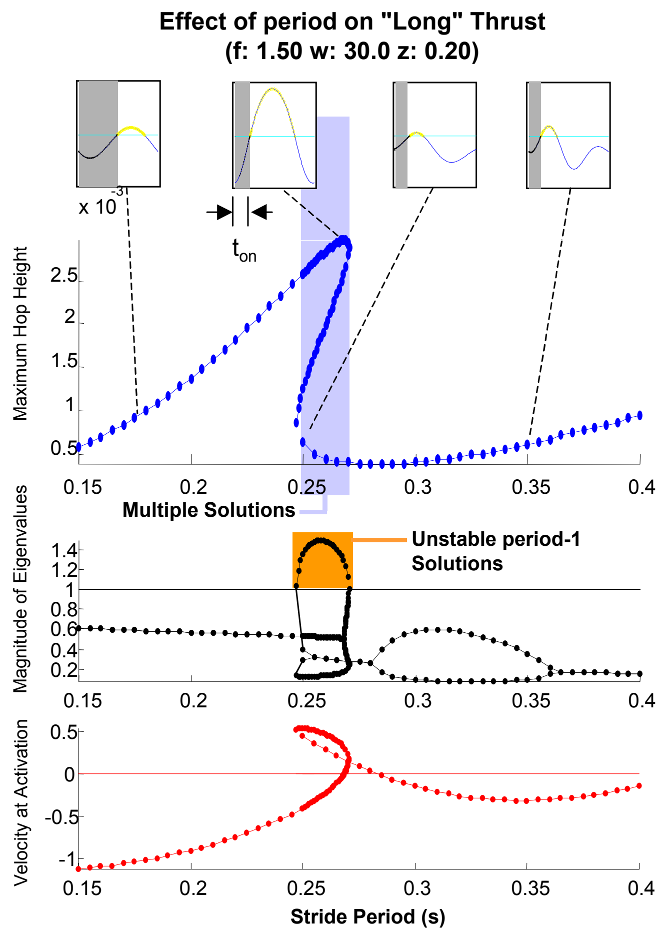

Figure 6. Effects of changing the stride period on steady-state motion and stability for the one-DOF hopper case in which thrust application ends at or after lift-off.

damping ratio, ζ. For short stride periods, hopping height starts out very small, as shown in the top plot. At these periods, thrust application starts well before maximum compression, given by the negative velocity at thrust application (in the figure, this velocity is normalized by the magnitude of the take-off velocity). These solutions are termed "Regular Hopping" as they represent a desired mode of hopping behavior. As the stride period is increased, hopping height increases, and velocity at application approaches zero. Finally, at a certain period (near 275ms period), height is maximized when velocity at application is nearly zero, as predicted. However, as the period approaches 275ms the magnitude of the eigenvalues quickly increases and the solution becomes unstable. Simulations of the hopper, though, never reach this point. As shown in the figure, other solutions to the state-steady conditions become available at a period near 250ms as the continuum of solutions folds back with respect to stride period. Of the two new sets of solutions available in this range of stride periods, one of them involves activating thrust after maximum compression and is unstable. The solutions in the second set are termed "Hop-settle-fire" as the mass has started to settle before thrust is applied. The hopping heights for these solutions are much lower, but their corresponding eigenvalues are also much lower, and the simulations converge to these solutions.

Figure 7 shows a typical example of the effects of changing the open-loop stride period for the "Short Thrust" case. For short periods, the solutions start out as "Regular Hopping." However, as the period is increased, the eigenvalues start to move outside the unit circle. Simulations for this range are "period-1 unstable" (the state does not repeat after one cycle), but tend to be "period-2 stable" (the state repeats after two cycles). As the period is further increased, the "Regular Hopping" solutions become period-1 stable again. The velocity at thrust activation also increases, and changes from negative (thrusting before maximum compression) to positive (thrusting after maximum compression). Maximum hopping height is also increased with period and keeps increasing until the continuum of solutions end. However, near 275ms period another continuum of valid steady-state solutions begins. This is again the "Hop-settle-fire" solution, for which hopping height is lower.

A rigorous analysis of the effects of the model's other parameters on the hopping motion is beyond the scope of this paper, but they are nonetheless stipulated here from experience with the simulations. The onset of the "Hop-settle-fire" solutions is determined largely by the system's natural frequency. These solutions become available when the period of thrust application is long enough that the system is allowed to settle according to its natural period. The addition of damping also makes these solutions possible, since without damping the system would not settle. Decreasing damping and increasing the thrust magnitude and duration all seem to have a destabilizing effect, as they extend the region of unstable solutions.

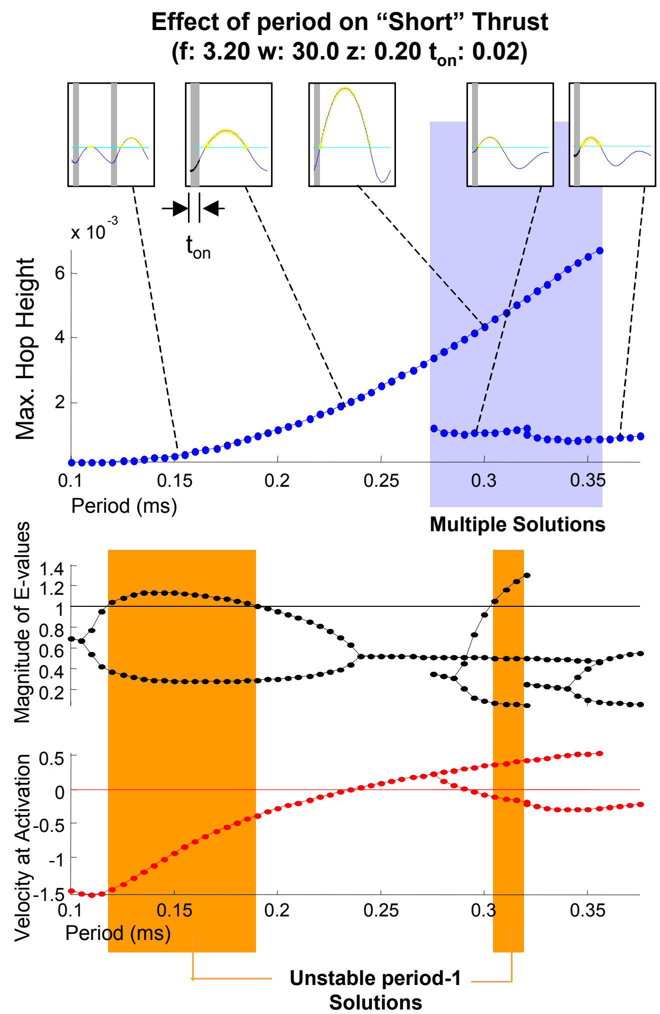

Figure 7. Effects of changing the stride period on steady-state motion and stability for the one-DOF hopper case in which thrust application ends before lift-off.

2.3 One-DOF model conclusions

From the analysis above, we draw the following observations which we postulate generalize to similar hopping systems with passive properties and an open-loop, clock-driven activation pattern:

1) For a wide range of activation periods, there exists one or more solutions to the steady-state conditions. These solutions may or may not be locally period-1stable. If there are multiple solutions for a given period, the system will tend to converge to the most stable solution, or may vacillate between equally stable solutions.

2) A given solution is such that the total amount of energy does not change within the stride period (the total amount of energy injected by the forcing function equals the total amount of energy passively dissipated). The magnitude and duration of the forcing function are given by the stride period and duty cycle of the open-loop activation pattern. Thus, a given solution will entail a phase difference between the forcing function and the motion of the system such that the forcing function may perform both positive and negative work.

3) The total amount of energy within a stride is maximized when the forcing function performs the most positive work, given by the force-velocity integral in Equation 3. With a fixed thrust magnitude, this integral depends primarily on the velocity at the start and end of thrust relative to the point of maximum compression.

4) In general, increasing the stride period tends to increase the velocity at both the start and end of activation and maximize the work input integral. However, as shown, this may result in instability (as in the "Long Thrust" case) or in "Hop-settle-fire" behavior, where the system settles to equilibrium between thrust periods.

These observations suggest that a good way to infer how effectively the actuator is being utilized is to monitor the start and end of thrust relative to the motion of the body. Since we are interested in using only simple sensors such as binary contact switches, we pay particular attention to the relationship between end of thrust activation and the end of the ground contact phase, or lift-off. The one-DOF analysis suggests that steady-state solutions in which the end of thrust occurs well before or after lift-off can be suboptimal in terms of the work input integral within one stride. This simple heuristic is explored and validated with experimental results of the multi-DOF hexapedal robot in the following section.

3. Stride Period Adaptation

3.1 Robot performance tests

The one-DOF model provided insight into the basic behavior of an open-loop hopping system with passive properties in terms of the work performed by the actuator and the resulting performance. In order to develop an adaptation law for the six-legged, multi-DOF robot, we must look at the factors that affect its performance and see whether the same basic mechanisms are evident. Figure 8 shows the performance results of the hexapedal robot as a function of open-loop stride period for three different cases. The dotted lines represent the results for a first prototype, here called robot 1, running on flat ground. The solid lines are for the same robot on flat ground, but with different actuators, here called robot 2. The new actuators are pneumatic pistons with faster air flow and less damping. Finally, the dashed lines are for robot 2 running on a 5 degree uphill slope. As shown in 8a, speed is maximized at different stride periods for different conditions, again motivating the need for adjustment or adaptation of the stride period. Although speed appears to be maximized for a range of stride periods, it is advantageous to use the largest possible stride period, since energy consumption is proportional to stride frequency.

Similar to the one-DOF model, the average magnitude of oscillations normal to the ground increases with stride period, as shown in 8b. However, at these higher periods, the motion was observed to be less period-1 stable, resulting in large non-periodic oscillations within each stride period. More indicative of the underlying dynamics is Figure 8c, which shows the average stride length (distance) as a function of stride period. As shown, stride lengths are maximized and remain fairly constant for large stride periods. Furthermore, this regime is associated with “Hop-settle-fire” behavior similar to the one observed in the one-DOF model, where the stride period is long enough that much of the energy from the previous hop is dissipated before thrust is initiated. As the stride period is decreased, the stride length begins to decrease. However, since speed is the product of stride length and stride frequency, decreasing the stride period results in the speed reaching a maximum near the point where the stride length starts to decrease, eventually dropping off for very short stride periods.

The quantities plotted so far, while indicative of the stride period needed for maximum speed, are difficult to measure proprioceptively (without external sensors) or without complex sensors (e.g. velocity sensors). For this reason, we examined the difference between the time that a particular tripod is deactivated, t_d (see Fig. 4), and the time that the middle-foot of that tripod leaves the ground, t_L, as suggested by the analysis of the one-DOF model. This quantity is plotted in Figure 8d for the different cases examined. This time delay, (t_d - t_L), is positive for long stride periods, which indicates that thrust application ends after lift-off, here caused by end-of-stroke or full extension. This delay also monotonically increases for longer periods since thrust application, or t_{on}, is set as a fixed percentage, or duty cycle, of the stride

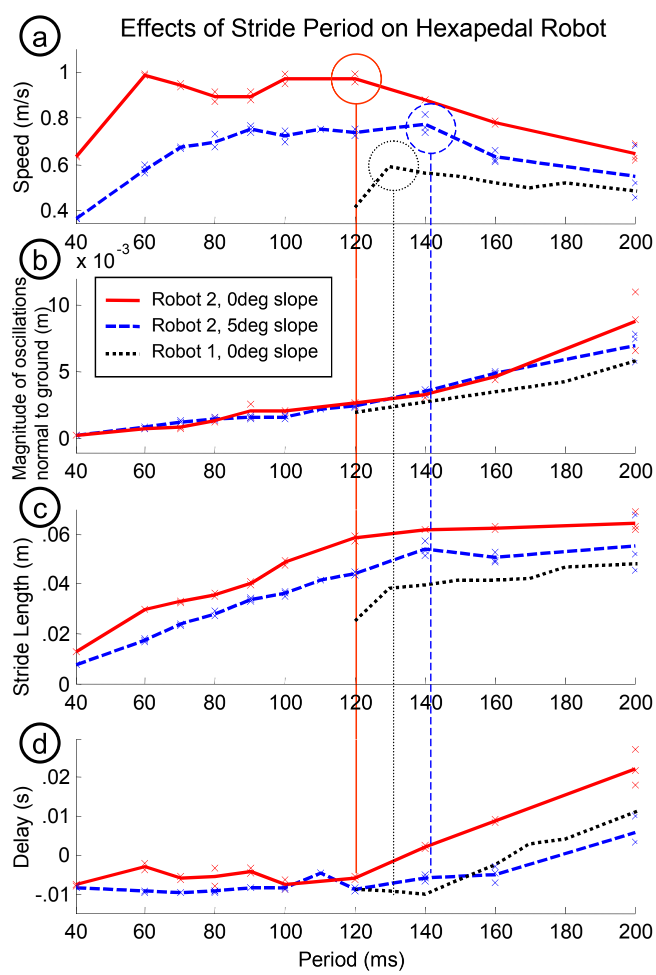

Figure 8. Performance tests for the hexapedal robot in flat ground and uphill terrain, as a function of open-loop stride period with constant duty cycle percentages.

period. Below a certain range of stride periods, however, the time delay is a nearly constant small negative value. In effect, deactivation of the tripod causes the spring-loaded leg pistons to retract and lose contact with the ground before full extension.

This change in the slope of the time delay (t_d - t_L) relative to the stride period occurs near the period for which stride length begins to decrease and ground speed is maximized. Although the dynamics of the robot's locomotion are affected by many factors, it appears that the amount of net positive work performed by the actuators, as indicated by the time delay (t_d - t_L), has a first-order effect in determining maximum ground speed. This correlation is used as the basis for the simple adaptation law described in the following section.

3.2 Adaptation strategy

The results from the previous sections motivate the robot stride period adaptation strategy described here. As illustrated by the one-DOF model, it is advantageous to use a stride period that results in a steady-state cycle in which thrust is deactivated near the point where full piston extension occurs in order to maximize work input. Similar to the one-DOF model, lower stride periods result in sub-optimal work input as thrust is terminated before full extension. Moreover, like the one-DOF model, higher stride periods result in "Hop-settle-fire" behavior and sometimes in period-1 unstable oscillations. A prototype adaptation law for maximizing ground speed that takes these findings into consideration using foot contact information is as follows:

$$\tau_{n+1} = \tau_n - K_p(t_d - t_L - t_v)$$

Here, K_p is the adaptation gain, t_v is a constant offset parameter, t_d is the time at which the valve is deactivated and t_L is the measured lift-off time of the middle-foot. Figure 9 illustrates what these quantities represent, where time is measured with respect to the initiation of the gait cycle, which starts when the valve for one of the tripods is activated. The adaptation law is based on contact information from a binary switch attached to the middle foot of the same tripod. The deactivation time t_d is determined by the stride period, τ, and duty cycle, which in this case is specified as a fixed percentage of the stride period. If there is no measured ground contact information, t_L, then the period is not modified.

Intuitively, this simple adaptation law can be described as trying to decrease the stride period as much as possible without exceeding the bandwidth of the actuators and without terminating the thrust application before full extension (to maximize available work). The stride period reaches an equilibrium value when $\Delta\tau$ is zero, which occurs when (t_d - t_L) is equal to the offset value, t_v. Since the delay (t_d - t_L) is nearly constant for lower stride periods, the offset value t_v is adjusted slightly above zero, so that the equilibrium stride period coincides with the change in slope of the delay (t_d - t_L) with respect to the stride period (see Figure 9).

3.3 Adaptation Results and Discussion

Figure 10 shows test results of the adaptation law implemented in the hexapedal robot 2 running on flat ground for several experiments in which the stride period was started at suboptimal values (see multimedia Extension 3). Figure 10a shows the ground speed of the robot as a function of time, and Figure 10b shows the stride period after each stride cycle, or learning loop, in which t_L was measured. The gain K_p was experimentally chosen to give the adaptation a fast learning rate while still achieving convergence. Note from Figure 10b that, although only a simple contact switch was used, the measured values of t_L are still prone to some noise, due to ground imperfections or disturbances to the robot, and adaptation does not necessarily proceed smoothly. This adaptation strategy was also shown to optimize speed in

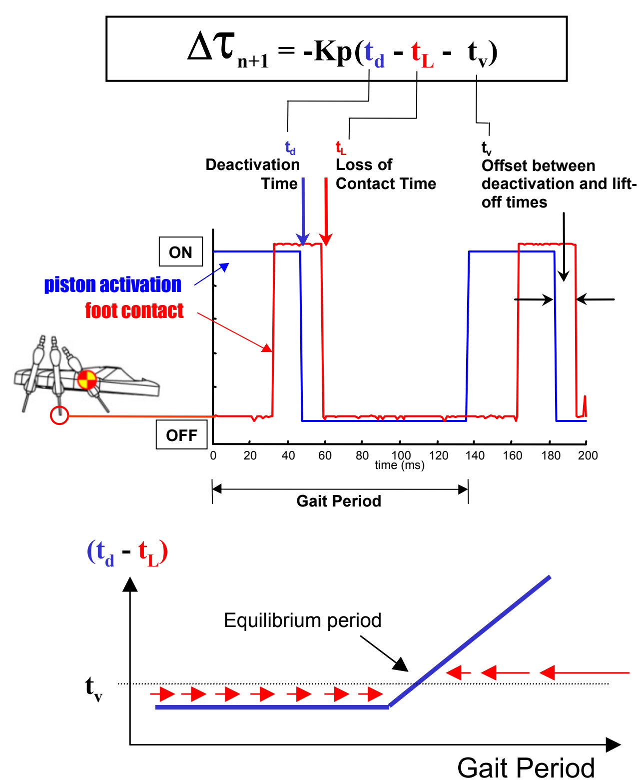

Figure 9. Simple gait period adaptation law based on the measured duration between foot contact events. A binary switch in the robot's middle foot provides contact information. This time duration is compared to the actuator valve deactivation time for the adaptation law.

robot 1, with different pneumatic pistons, and for the case where the input actuator pressure was decreased in robot 2 by 13% (shown in Figure 11).

For an uphill ground slope of 5 degrees, the adaptation strategy also converges to an equilibrium stride period, as shown in Figure 12 (see multimedia Extension 4). This new equilibrium period (~170ms) is higher than the equilibrium period for flat ground running (~110ms) and results in faster uphill running than with the optimal period for flat ground. However, the new equilibrium period is somewhat higher than the period found to be optimal at 5 deg. slopes (~140ms). This indicates that, although it works to improve locomotion speed when transitioning to sloped terrain, the simple threshold-based adaptation law implemented here results in errors in the optimal equilibrium stride period for uphill running. This is mainly attributed to the gradual change in slope in the plot of (t_d - t_L) for 5 deg uphill terrain compared to the prominent "kink" in the corresponding plot for flat terrain (see Figure 8). The use of a threshold to detect this change in slope results in equilibrium periods that are longer than optimal. Future work will experiment with more sophisticated ways to detect this change in slope. Furthermore, the factors that affect uphill running may need to be re-examined. For example, in seeking to increase the stride frequency for optimal ground speed in flat terrain, the prototype adaptation law presented here reduces oscillations in the direction normal to the ground, which we believe may have a significant role while climbing up-hill terrain.

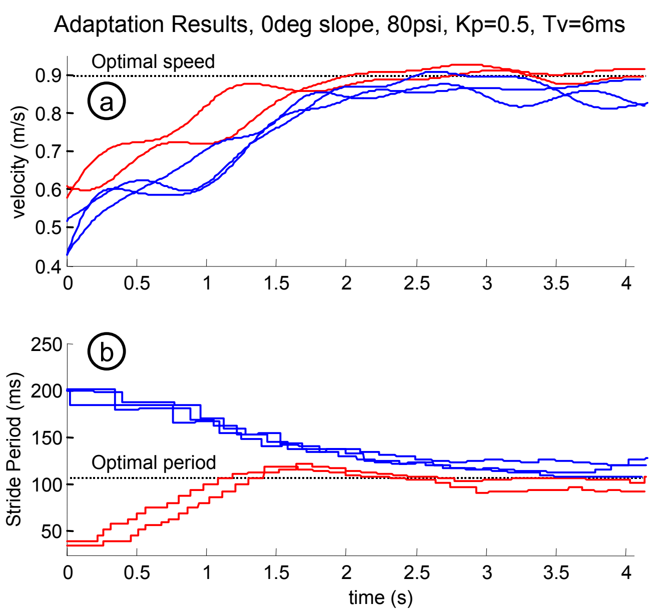

Figure 10. Adaptation results for flat terrain (dashed lines are approximate optimal values established empirically). The figures show the ground speed of the robot and the stride period as it is adapted from suboptimal starting conditions.

4. Conclusions and Future Work

The analyses and experiments in the previous sections show that for an open-loop running robot, stride frequency and thrust duration are important parameters that govern hop height and forward speed. The single legged hopper model

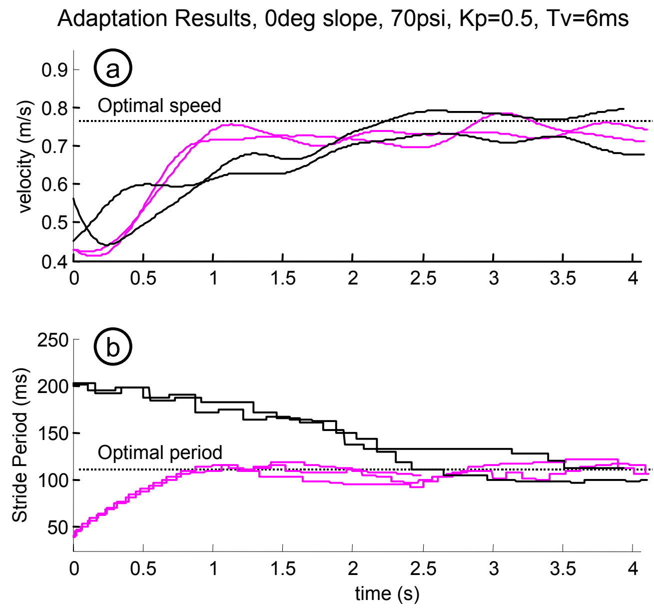

Figure 11. Adaptation results for flat terrain with a 13% decrease in pneumatic actuator input pressure. The adaptation optimizes ground speed by converging to a slightly higher stride period than in Figure 10.

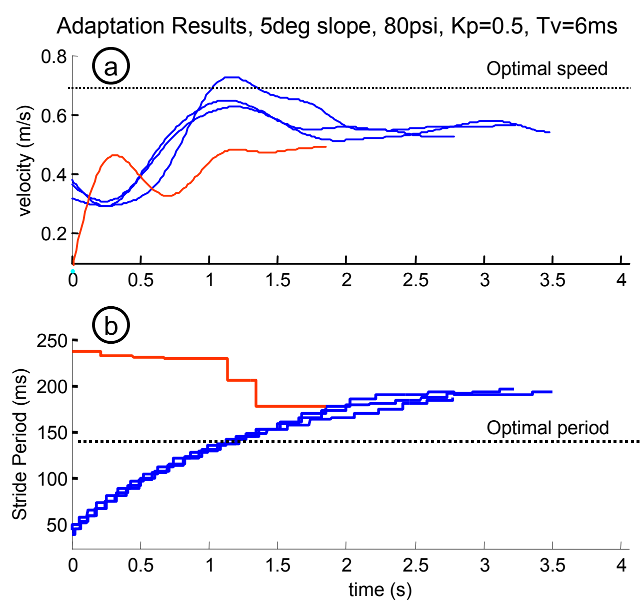

Figure 12. Adaptation results for an uphill slope of 5 degrees. The adaptation strategy improves the locomotion, but converges to a stride period slightly higher than the optimal stride period.

reveals that optimal hop height is obtained by maximizing the product of thrust force and velocity over the thrust duration. However, this product is subject to both dynamic constraints and hardware limitations. The dynamic constraints include the requirement of a stable, steady-state periodic solution to which the system will converge. Significant passive damping, as found in insects and in robots like Sprawlita, increases the regime of stable, periodic operation with open-loop forcing. The hardware limitations include the stroke length, the speed at which the piston can be filled and exhausted and the maximum thrust force available.

An adaptation strategy for the stride period that takes these limitations into account and tries to optimize ground speed was presented in this paper. The adaptation law seeks to obtain the most work from the actuators without exceeding their bandwidth. This adaptation law uses only the sensed duration of ground contact during each stride, and was shown to cause the stride period to converge to optimal values for a range of robot-to-robot variations and operating pressures. When making the transition from level to uphill running, the robots converge to slightly suboptimal values of stride period and velocity. The difficulty in this case is that the transition between optimal and over-long periods is less distinct and less easily identified with a simple threshold test. More sophisticated detection of the transition is an area of ongoing work.

More generally, the adaptation scheme presented in this paper is an example of an approach that is particularly well suited for small, biomimetic robots by requiring no expensive or sophisticated sensing or feedback. In this case, only simple binary switches are needed to provide an estimate of ground contact time. The adaptation scheme takes advantage of the passive properties of the robot that allow it to run stably over a range of open-loop stride frequencies and actuator duty cycles. In the event of sensor failure, the performance of the robot degrades only to that of the open-loop system without adaptation. This approach allows the robots to remain simple, inexpensive and robust while also being able to "tune" themselves to accommodate individual variabilities and changes in operating conditions.

Future work will build upon the simple adaptation law tested in this paper to incorporate other simple sensor information (e.g. tilt sensor, contact switches in other feet) in order to increase performance and adaptability. As discussed previously, further understanding of the robot's dynamic interaction with different types of terrain such as sloped or compliant surfaces will allow us to increase the adaptation's versatility. Finally, future work will study the effects of such an adaptation law on other types of behavior, such as rapid turning and navigation.

5. Acknowledgments

We have been fortunate to collaborate with Professor Robert J. Full at the U.C. Berkeley Polypedal Laboratory throughout this work and to benefit from his prodigious knowledge and understanding of the mechanisms underlying insect locomotion. We are also grateful for lengthy discussions on adaptation with Dr. Goran Djordevic at the Johns Hopkins' Laboratory for Human Motor Learning. Thanks also to Jonathan Clark, Sean Bailey, Edward Froehlich and the other members of the Biomimetics team at CDR. Funding was provided by the Office of Naval Research under grant N00014-98-1-0669. Jonathan Karpick is supported by an Alex and Brit d'Arbeloff Stanford Graduate Fellowship.

6. References

Ahn, A N; Full, R J. 1997. "A motor and a brake: Similar EMGs in two adjacent leg extensor muscles result in completely different function." American Zoologist. 37:107A.

Bailey, S. A., Cham, J. G., Cutkosky, M. R., and Full, R. J., "Biomimetic Mechanisms via Shape Deposition Manufacturing," in Robotics Research: the 9th International Symposium, J. Hollerbach and D. Koditschek (Eds), Springer-Verlag, London, 1999.

Berkemeier, M. D. and Desai, K.V., "A Comparison of Three Approaches for the Control of Hopping Height in Legged Robots." Submitted to the International Journal of Robotics Research, 1998.

Cham, J. G., Bailey, S. A., Clark, J. E., Full, R. J. and Cutkosky, M. R., "Fast and Robust: Hexapedal Robots via Shape Deposition Manufacturing," International Journal of Robotics Research (In press).

DeCarlo, R., Branicky, M., Pettersson, S., and Lennartson B., "Perspectives and Results on the Stability and Stabilizability of Hybrid Systems" Proceedings of the IEEE, July 2000, pp. 1069-1082.

Full, R.J., Autumn, K., Chung, J.I., Ahn, A., "Rapid negotiation of rough terrain by the death-head cockroach." American Zoologist. 38:81A. 1998.

Garcia, M., Kuo, A., Peattie, A. M., Wang, P. C. and Full, R. J., "Damping and Size: Insights and Biological Inspiration" in Proc. of the Intl. Symp. on Adaptive Motion of Animals and Machines, Montreal, Canada, August 2000.

Koditschek, D. E. and Buhler, M., "Analysis of a Simplified Hopping Robot," International Journal of Robotics Research, 10:6, 587-605. 1991.

Komsuoglu, H. and Koditschek, D. E., "Preliminary Analysis of a Biologically Inspired 1-DOF 'Clock' Stabilized Hopper", Proceedings of World Multiconference on Systemics, Cybernetics and Informatics (SCI2000), Orlando, USA, July 23-26, 2000, Vol IX, pp 670-675.

Kubow, T.M., Full, R.J., "The role of the mechanical system in control: A hypothesis of self-stabilization in hexapedal runners." Phil. Trans. Roy. Soc. London B. 354, 849-862. 1999.

Meijer, K., Full, R.J., "Stabilizing properties of invertebrate skeletal muscle." American Zoologist. In press.
Raibert, M. H., "Legged robots that balance." MIT Press, Cambridge, MA, 1986.
Ringrose, R., "Self-stabilizing running," IEEE ICRA Proceedings, Albuquerque, NM, 1997.
Sastry, S. "Nonlinear Systems: Analysis, Stability and Control". Springer Verlag. 1999.

Appendix

Equations of Motion

The equations of motion for the one-DOF hopper in Figure 4 can be written, in normalized coordinates, as:

$$\dot{X} = AX + B$$

where A and B are defined as:

$$\left.A = \begin{bmatrix} 0 & 1 \\ -w^2 & -2\zeta w \end{bmatrix} \quad B = \begin{bmatrix} 0 \\ f(t) - 1 \end{bmatrix}\right\} \qquad (x \le 0)$$

during the stance, or ground-contact phase, and:

$$\left.A = \begin{bmatrix} 0 & 1 \\ 0 & 0 \end{bmatrix} \quad B = \begin{bmatrix} 0 \\ -1 \end{bmatrix}\right\} \qquad (x > 0)$$

during the airborne, or ballistic, phase. w is the natural frequency and ζ is the damping ratio of the mass-spring-damper system. The thrust force $f(t)$ is determined by the open-loop motor control pattern:

$$f(t) = \begin{cases} T_n & t_{off} < t \le t_{off} + t_{on} \\ 0 & otherwise \end{cases}$$

where T_n is the normalized thrust magnitude. Here, t is reset to $t=0$ when t reaches τ. This system is treated as a piecewise affine linear hybrid dynamic system with continuity of state at the mode transitions (Branicky, et al., 2000). The three modes are termed "AIR" (airborne phase), "ON" (stance phase with active thrust) and "OFF" (stance phase with zero thrust). The time solutions of the state vector $X(t)$ for the three modes are:

$$\begin{aligned} &AIR \quad X(t) = \begin{bmatrix} 1 & t \\ 0 & 1 \end{bmatrix} X_0 - \begin{bmatrix} t^2/2 \\ t \end{bmatrix} \\ &ON \quad X(t) = e^{At}(X_0 - X_{eon}) + X_{eon} \\ &OFF \quad X(t) = e^{At}(X_0 - X_{eoff}) + X_{eoff} \end{aligned}$$

Here, X_o is the state at the beginning of each mode and X_{eon} and X_{eoff} are the equilibrium states for each of the stance modes:

$$X_{eon} = \begin{bmatrix} \dfrac{T_n - 1}{w^2} \\ 0 \end{bmatrix} \qquad X_{eoff} = \begin{bmatrix} -\dfrac{1}{w^2} \\ 0 \end{bmatrix}$$

Return Maps

In order to study the steady-state motion and local stability of the hopper, we define a return map $F(X_n)$ based on the state at thrust application, X_n (Sastry, 1999). Since mode switches are both a function of the state and of the open-loop motor pattern, the system trajectory can undergo an indeterminate number of sequences of mode changes. In this analysis, we consider the two hopping behaviors characterized as "Long Thrust" and "Short Thrust." In "Long Thrust," we assume that the hopper lands and activates thrust during stance, and that the thrust application duration is long enough to continue until or past lift-off, such that the mode sequence is ON-AIR-OFF. In "Short Thrust," we assume that the hopper lands and also activates thrust during stance, but that thrust application ends before lift-off, such that the mode sequence is ON-OFF-AIR-OFF.

For "Long Thrust," we introduce the two timing variables t_{on} (duration of active thrust application) and t_a (1/2 the duration of the airborne phase). To derive the return map, we take advantage of the facts that the take-off velocity (velocity at the ON-AIR mode transition) is the negative of the landing velocity (velocity at the AIR-OFF mode transition) and that this velocity is, in normalized coordinates, equal to t_a. We also take advantage of the fact that the total duration of the modes must equal τ. The return map can then be found by nesting the time solutions for the individual modes in the ON-AIR-OFF sequence:

$$\begin{aligned} X_{n+1} = F(X_n) = X_{eoff} - e^{A(\tau - 2t_a - t_{on})}(X_{eon} + X_{eoff}) \ldots \\ -e^{A(\tau - 2t_a)}(X_n - X_{eon}) \end{aligned}$$

In order to find the steady-state solutions, or "fixed points," we impose the constraint $X_{takeoff} = -X_{landing} = [0\ t_a]^T$ and seek an expression with only two unknowns:

$$\begin{aligned} X_{takeoff} = e^{A(t_{on} + t_{off})}(X_{touchdown} - X_{eoff}) + \ldots \\ e^{At_{on}}(X_{eoff} - X_{eon}) + X_{eon} = -X_{touchdown} \end{aligned}$$

which implies:

$$\begin{aligned} X_{takeoff} + e^{A(t_{on} + t_{off})}(X_{takeoff} + X_{eoff}) + \ldots \\ e^{At_{on}}(X_{eon} - X_{eoff}) - X_{eon} = \begin{bmatrix} 0 \\ 0 \end{bmatrix} \end{aligned}$$

This set of equations is solved numerically, where our solution vector is $[t_{on} \quad t_a]$. If a solution exists, it may be unique or there may be multiple solutions. Once found, the solution $[t_{on}^* \quad t_a^*]$ can be used to find X^*, which satisfies:

$$X^* = F(X^*)$$

The return map for the "Short Thrust" mode sequence is similarly found by nesting the time solutions in the ON-OFF-AIR-OFF sequence. Here, we introduce the variables t_{o1} (duration of first OFF stance mode), t_a (1/2 the duration of the airborne phase) and t_{o2} (duration of the second OFF stance mode). The parameter t_{on} is a constant in this case. Again, taking advantage of the fact that the total time duration of the modes must equal τ, the return map is found as:

$$X_{n+1} = F(X_n) = X_{eoff} - 2e^{A(\tau - 2t_a - t_{on} - t_{o1})}X_{eoff} - \ldots$$
$$e^{A(\tau - 2t_a - t_{on})}(X_{eon} - X_{eoff}) - e^{A(\tau - 2t_a)}(X_n - X_{eon})$$

Similarly, imposing the steady state constraint, $X_{takeoff} = -X_{landing}$, and going from OFF ($t_{o2}$) to ON ($t_{on}$) to OFF ($t_{o1}$) modes, we can write the equations as:

$$X_{takeoff} = e^{A(\tau - 2t_a)}(X_{touchdown} - X_{eoff}) + \ldots$$
$$e^{A(t_{on} + t_{o1})}(X_{eoff} - X_{eon}) + e^{At_{o1}}(X_{eon} - X_{eoff}) + X_{eoff} = \ldots$$
$$-X_{touchdown}$$

which implies:

$$X_{takeoff} + e^{A(\tau - 2t_a)}(X_{takeoff} + X_{eoff}) - \ldots$$
$$e^{A(t_{on} + t_{o1})}(X_{eoff} - X_{eon}) - e^{At_{o1}}(X_{eon} - X_{eoff}) - X_{eoff} = \begin{bmatrix} 0 \\ 0 \end{bmatrix}$$

This is again solved numerically using a solution vector $[t_{o1} \quad t_a]$. As in the previous case, multiple solutions may exist, and it is possible a solution does not exist. Again, if a solution is found, t_{o1}^* and t_a^* can be used to find X^* using the appropriate time solutions.

Local Stability

The local stability of a particular steady-state solution, or fixed point X^*, can be determined by evaluating the Jacobian of the return map at the fixed point, and studying its eigenvalues (Sastry, 1999). The Jacobian, termed M, maps perturbations about the fixed point, δX_n, on one cycle, to perturbations about the fixed point on the next cycle, δX_{n+1}. Therefore, if the eigenvalues of the Jacobian evaluated at X^* are less than unity, the perturbations will decay, which indicates a locally stable steady-state solution:

$$|eig(M(X^*))| < 1$$

where M is defined as:

$$M(X_n) = \frac{\partial}{\partial X_n}F(X_n)$$

In order to obtain this multi-variable derivative, we take advantage of the derivative properties of the matrix exponential:

$$\frac{\partial e^{Af(s)}}{\partial s} = Ae^{Af(s)}\frac{\partial f}{\partial s} = e^{Af(s)}A\frac{\partial f}{\partial s}$$

where s is a scalar variable and f a scalar function.

Thus, the Jacobian matrix for the "Long Thrust" case is found to be:

$$M(X^*) = \frac{\partial}{\partial X_n}F(X^*) = 2A(X_{eoff} - X^*)\left.\frac{\partial t_a}{\partial X_n}\right|_{X^*} + \ldots$$
$$Ae^{At_{off}^*}(X_{eon} + X_{eoff})\left.\frac{\partial t_{on}}{\partial X_n}\right|_{X^*} - e^{A(\tau^* - 2t_a^*)}$$

where the expression has been simplified by using the steady state condition that $X^* = F(X^*)$. In order to find the expressions $\partial t_a/(\partial X_n)$ and $\partial t_{on}/(\partial X_n)$, we use the take-off condition:

$$\begin{bmatrix} 0 \\ t_a \end{bmatrix} = e^{At_{on}}(X_n - X_{eon}) + X_{eon}$$

and take derivatives with respect to X_n to find:

$$\begin{bmatrix} 0 \quad 0 \\ \partial t_a/\partial X_n \end{bmatrix} = Ae^{At_{on}}(X_n - X_{eon})\frac{\partial t_{o1}}{\partial X_n} + e^{At_{on}}$$

Decomposing each row and rearranging to solve for $\partial t_a/(\partial X_n)$ and $\partial t_{on}/(\partial X_n)$ yields:

$$\left.\frac{\partial t_{on}}{\partial X_n}\right|_{X^*} = -\left[\begin{bmatrix} 1 & 0 \end{bmatrix} Ae^{At_{on}^*}(X^* - X_{eon})\right]^{-1}\begin{bmatrix} 1 & 0 \end{bmatrix} e^{At_{on}^*}$$

$$\left.\frac{\partial t_a}{\partial X_n}\right|_{X^*} = \begin{bmatrix} 0 & 1 \end{bmatrix} e^{At_{on}^*}\left[A(X^* - X_{eon})\left.\frac{\partial t_{on}}{\partial X_n}\right|_{X^*} + I\right]$$

Similarly, the Jacobian matrix for the "Short Thrust" case has been found to be:

$$M(X^*) = \frac{\partial}{\partial X_n}F(X^*) = 2A(X_{eoff} - X^*)\left.\frac{\partial t_a}{\partial X_n}\right|_{X^*} + \ldots$$
$$2Ae^{A(\tau - 2t_a - t_{on} - t_{o1})^*}(X_{eoff})\left.\frac{\partial t_{o1}}{\partial X_n}\right|_{X^*} - e^{A(\tau^* - 2t_a^*)}$$

where $\partial t_a/(\partial X_n)$ and $\partial t_{o1}/(\partial X_n)$, are found by using the take-off condition:

$$\begin{bmatrix}0\\ t_a\end{bmatrix} = e^{A(t_{on}+t_{o1})}(X_n - X_{eon}) + e^{At_{o1}}(X_{eon} - X_{eoff}) + X_{eoff}$$

and taking the derivatives with respect to X_n:

$$\begin{bmatrix}0\ 0\\ \partial t_a/\partial X_n\end{bmatrix} = Ae^{At_{o1}}[e^{At_{on}}(X^* - X_{eon}) + \ldots$$

$$X_{eon} - X_{eoff}]\frac{\partial t_{o1}}{\partial X_n}\bigg|_{X^*} + e^{A(t_{on}+t_{o1})}$$

Decomposing each row and rearranging to solve for $\partial t_{o1}/(\partial X_n)$ and $\partial t_a/(\partial X_n)$ yields:

$$\frac{\partial t_{o1}}{\partial X_n}\bigg|_{X^*} = -\left[\begin{bmatrix}1 & 0\end{bmatrix} A e^{At_{o1}^*}[e^{At_{on}}(X^* - X_{eon}) + X_{eon} - X_{eoff}]\right]^{-1} \cdots$$

$$\begin{bmatrix}1 & 0\end{bmatrix} e^{At_{on}^*}$$

$$\frac{\partial t_a}{\partial X_n}\bigg|_{X^*} = \begin{bmatrix}0 & 1\end{bmatrix}\left[Ae^{At_{on}}(X_n - X_{eon})\frac{\partial t_{o1}}{\partial X_n} + e^{At_{on}}\right]$$

Using these expressions for the Jacobian, we can determine the local stability of a particular fixed point by first evaluating the Jacobian at the fixed point and then finding its eigenvalues.

Index to Multimedia Extensions

The multi-media extensions to this article in review can be found online at *http://cdr.stanford.edu/biomimetics/documents/ijrr2002/captions.html*.

Table 1: Multimedia Extensions

Extension	Media Type	Description
1	video	Video showing "Sprawlita" running despite large disturbances. This disturbance rejection is accomplished without sensory feedback through the robot's passive properties and open-loop control.
2	video	Video showing "Sprawlita" overcoming hip-height obstacles.
3	video	Video showing sample results of implementing the adaptation strategy based on binary contact information from a switch in one the robot's feet. The video shows experiments on flat ground in which the robot's stride period was started at suboptimal values.
4	video	Video sample results of the adaptation strategy on an uphill slope of 5 degrees. The video shows experiments in which the robot's stride period was started at suboptimal values.